












AtPRMT5-mediated AtLCD methylation improves Cd²⁺ tolerance via increased H₂S production in Arabidopsis

Haiyan Cao ¹, Yali Liang ¹, Liping Zhang ¹, Zhiqiang Liu ¹, Danmei Liu ¹, Xiaofeng Cao ², Xian Deng ^{2,*}, Zhuping Jin ^{1,*} and Yanxi Pei ^{1,*}

- 1 School of Life Science and Shanxi Key Laboratory for Research and Development of Regional Plants, Shanxi University, 030006 Taiyuan, China
2 State Key Laboratory of Plant Genomics and National Center for Plant Gene Research, Institute of Genetics and Developmental Biology, Chinese Academy of Sciences, 100101 Beijing, China

*Author for correspondence: peiyanxi@sxu.edu.cn (Y.P.), jinzhuping@sxu.edu.cn (Z.P.), xdeng@genetics.ac.cn (X.D.)

Y.P., Z.J., and X.D. conceived and directed the project. H.C., L.Z., Y. L., and Z.L. performed the experiments. H.C., Y.L., and D.L. analyzed the data. Y.P., Z.J., X.D., and H.C. wrote the manuscript. X.C. supervised the project and revised the manuscript. All authors read and approved the final manuscript. The author responsible for distribution of materials integral to the findings presented in this article in accordance with the policy described in the Instructions for Authors (<https://academic.oup.com/plphys/pages/general-instructions>) is: Yanxi Pei (peiyanxi@sxu.edu.cn).

Abstract

Arabidopsis (*Arabidopsis thaliana*) PROTEIN ARGININE METHYLTRANSFERASE5 (PRMT5), a highly conserved arginine (Arg) methyltransferase protein, regulates multiple aspects of the growth, development, and environmental stress responses by methylating Arg in histones and some mRNA splicing-related proteins in plants. Hydrogen sulfide (H₂S) is a recently characterized gasotransmitter that also regulates various important physiological processes. L-cysteine desulfhydrase (LCD) is a key enzyme of endogenous H₂S production. However, our understanding of the upstream regulatory mechanisms of endogenous H₂S production is limited in plant cells. Here, we confirmed that AtPRMT5 increases the enzymatic activity of AtLCD through methylation modifications during stress responses. Both *atprmt5* and *atlcd* mutants were sensitive to cadmium (Cd²⁺), whereas the overexpression (OE) of *AtPRMT5* or *AtLCD* enhanced the Cd²⁺ tolerance of plants. AtPRMT5 methylated AtLCD at Arg-83, leading to a significant increase in AtLCD enzymatic activity. The Cd²⁺ sensitivity of *atprmt5-2 atlcd* double mutants was consistent with that of *atlcd* plants. When *AtPRMT5* was overexpressed in the *atlcd* mutant, the Cd²⁺ tolerance of plants was significantly lower than that of *AtPRMT5*-OE plants in the wild-type background. These results were confirmed in pharmacological experiments. Thus, AtPRMT5 methylation of AtLCD increases its enzymatic activity, thereby strengthening the endogenous H₂S signal and ultimately improving plant tolerance to Cd²⁺ stress. These findings provide further insights into the substrates of AtPRMT5 and increase our understanding of the regulatory mechanism upstream of H₂S signals.

Introduction

Hydrogen sulfide (H₂S) has been identified as a gasotransmitter, together with nitric oxide and carbon monoxide, and it participates in a wide range of physiological processes (Wang, 2002). In plants, H₂S is involved in seed germination,

root morphogenesis, stomatal movement, and photosynthesis (Zhang et al., 2009, 2020a; Zhou et al., 2018; Chen et al., 2020; Shen et al., 2020). Moreover, H₂S participates in response to many abiotic stresses, including drought, salt, low temperature, and osmotic stresses, resulting in research

interest (Jin et al., 2013; Corpas, 2019; Liu et al., 2019; Jiang et al., 2020).

Cadmium (Cd) is a kind of environmental pollutant that has serious adverse impacts on plants. Through crops, Cd easily infiltrates the food chain, and it is seriously harmful to human and animal health (Buchet et al., 1990). In plants, Cd stress causes a series of morphological and physiological changes, such as leaf chlorosis, leaf curl, inhibited root elongation, biomass reduction, stomatal closure, imbalanced water absorption, and inhibited photosynthesis (Clemens, 2006; Clemens and Ma, 2016).

H₂S can effectively enhance the tolerance to Cd stress in various plants. For example, under Cd²⁺-stress conditions, an exogenous H₂S pretreatment can affect the relative absorptions of K⁺ and Ca²⁺ and increase photosynthesis and antioxidant enzymatic activities to alleviate damage in *Nicotiana benthamiana* seedlings (Wang et al., 2021). H₂S can stimulate the activities of AsA-GSH cycle enzymes in tomato (*Solanum lycopersicum* L.) (Alamri et al., 2020) or participate in salicylic acid production in Arabidopsis (Qiao et al., 2015) to improve its Cd²⁺ tolerance. In addition, H₂S can reduce ROS accumulation and inhibit Cd²⁺-induced root tip cell death in cucumber (*Cucumis sativus* L.) and Chinese cabbage (*Brassica rapa* L. ssp. *pekinensis*) by activating the antioxidant system (Zhang et al., 2015; Luo et al., 2020).

In plants, L-cysteine desulphydrase (LCD) and D-cysteine desulphydrase (DCD) are important H₂S-generating enzymes that can degrade cysteine (Cys) into H₂S, NH₃, and pyruvate (Riemenschneider et al., 2005; Papenbrock et al., 2007). The transcriptional expression of *LCD* and *DCD* is up-regulated by Cd²⁺ stress (Cui et al., 2014; Zhang et al., 2015; Lv et al., 2017). Under Cd²⁺-stress conditions, an *atlcd* mutant shows greater Cd²⁺ sensitivity, whereas the phenotype of *AtLCD*-overexpressing (OE) Arabidopsis plants is the opposite (Qiao et al., 2015). Some factors regulating the expression of H₂S generating genes have been reported. The TGA3 factor binds to the *AtLCD* promoter region and activates its expression, thereby increasing the production of H₂S (Fang et al., 2017). Similarly, the trans-factor WRKY13 binds to the promoter of *AtDCD* and upregulates its expression (Zhang et al., 2020b). In general, our understanding of the upstream regulatory mechanisms of H₂S production is still very limited. In particular, whether the LCD activity can be regulated at the post-translational level is still not known.

Protein Arg methylation is an important post-translational modification. It is involved in different key biological processes, including RNA processing, DNA repair, and signal transduction, and it is considered an epigenetic regulator of transcription (Bedford and Richard, 2005; Bedford and Clarke, 2009). This modification is catalyzed by a group of protein Arg methyltransferases (PRMTs) that are divided into types I and II on the basis of biochemical activity (Blanc and Richard, 2017). PROTEIN ARGININE METHYLTRANSFERASE5 (PRMT5) (At4g31120), also known as SKB1, mediates the symmetric Arg dimethylation and is the most critical member of this family (Wang et al., 2007).

PRMT5 is involved in the regulation of plant growth and development, including the growth rate, flowering time, root development, circadian rhythm, and bud regeneration (Pei et al., 2007; Wang et al., 2007; Schmitz et al., 2008; Hong et al., 2010; Sanchez et al., 2010; Li et al., 2016; Liu et al., 2016a). PRMT5 also plays critical roles in the perception of environmental cues by plants, including abiotic stresses and vernalization. An *atprmt5* mutant shows a high salt sensitivity. Under salt-stress conditions, AtPRMT5 was dissociated from the chromatin. Thus, the level of H4R3sme2 decreased, which induced stress response gene expression. In addition, the methylation level of the small nuclear ribonucleoprotein Sm-like4 (LSM4) increased, which then affected the splicing of stress-response genes (Zhang et al., 2011). In Arabidopsis, AtPRMT5-mediated histone H4R3 dimethylation negatively regulates iron homeostasis. The buds of *atprmt5* mutants accumulate more iron and show an insensitivity to iron deficiency (Fan et al., 2014). The gasotransmitter nitric oxide increases the methyltransferase activity of AtPRMT5 by increasing its S-nitrosylation level, which improves the plant's abiotic stress tolerance (Hu et al., 2017). Further, AtPRMT5 mediates the methylation of AtSMD1, D3, U small nuclear ribonucleoproteins, and AtLSM4 proteins, leading to changes in gene alternative splicing. To date, these are the main known functional modes of PRMT5. It still remains to be determined whether there are enzymatic proteins that are direct substrates of PRMT5.

The biological regulatory functions of PRMT5 overlap with those of H₂S, especially in abiotic stress responses. This implied an interaction between them. In this study, we detail a pathway in which AtPRMT5 regulates endogenous H₂S production and improves heavy metal tolerance through the direct methylation of AtLCD. This is an important discovery that AtPRMT5 directly regulates enzymatic activity through methylation. In addition, we show a regulatory pathway for endogenous H₂S emission in plants.

Results

Either AtLCD or AtPRMT5 can improve Cd²⁺ tolerance in Arabidopsis

LCD enhances plant tolerance when exposed to various abiotic stresses, including drought, salt, high temperature, and heavy metals (Li et al., 2013; Scuffi et al., 2014; Chen et al., 2015; Zhao et al., 2018). To confirm the role of AtLCD in the regulation of Cd²⁺ tolerance, the *AtLCD* transcript level was determined in wild type (WT) under Cd²⁺-stress conditions. *AtLCD* was induced after 6 h, but did not peak until 12 h (Figure 1A). Consequently, we obtained and identified 35S::*AtLCD* transgenic plants and the T-DNA insertion mutant *atlcd* (Supplemental Figures S1 and S2). WT, *atlcd*, *AtLCD*-OE1, and *AtLCD*-OE2 seedlings were cultured on 1/2 Murashige and Skoog (MS) medium with or without Cd²⁺ for 14 days, and the half-inhibition concentration of Cd²⁺ was used for screening, as shown in Supplemental Figure S3. The root lengths of seedlings were also analyzed after

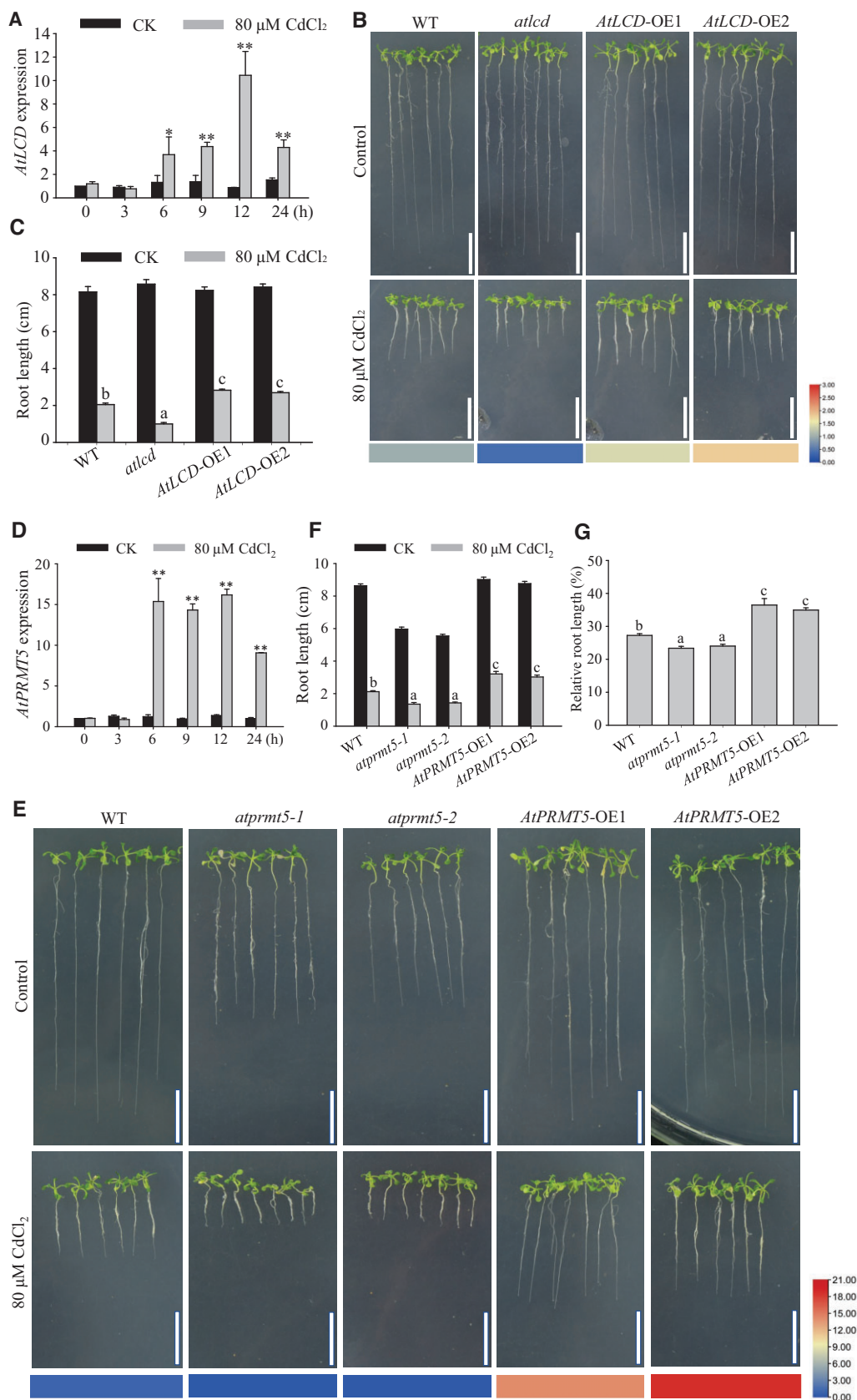


Figure 1 Phenotypic analysis of different plant materials exposed to Cd²⁺ stress. A, RT-qPCR analysis of *AtLCD* in WT with (gray column) or without (black column) Cd²⁺ stress. RNA was extracted from 10-day-old plants exposed to 80 μ M CdCl₂ for 0, 3, 6, 9, 12, and 24 h. *AtACT2* was used as the internal control. Error bars represent SEs, $n = 3$. B and C, Analysis of the Cd²⁺ tolerance of WT, *atlcd*, *AtLCD-OE1*, and *AtLCD-OE2* seedlings grown on 1/2 MS medium. B, Phenotype of seedlings at 14 days without (top panels) and with (bottom panels) the 80 μ M CdCl₂ treatment; scale

(continued)

14 days. There was no substantial phenotypic difference among different plant lines under normal growth conditions. In Cd^{2+} -containing medium, the *AtLCD*-OE1 and *AtLCD*-OE2 plants exhibited a higher tolerance to Cd^{2+} , whereas *atlcd* plants had a Cd^{2+} -sensitive phenotype compared with WT (Figure 1B). The root lengths of *AtLCD*-OE1 and *AtLCD*-OE2 plants were greater compared with that of the WT (Figure 1C). There was a substantially positive association between root length phenotype and *AtLCD* gene expression (Figure 1B, Heat map).

Mutations in *AtPRMT5* may cause developmental defects and increase sensitivity in response to abiotic stress in plants (Pei et al., 2007; Zhang et al., 2011; Hu et al., 2017). Thus, we investigated whether *AtPRMT5* is involved in Cd^{2+} -stress responses. Similarly, the expression of *AtPRMT5* started to increase after treating with Cd^{2+} for 6 h and continued until 24 h (Figure 1D). Subsequently, to further confirm the function of *AtPRMT5* in Cd^{2+} -stress responses, we constructed 35S::*AtPRMT5* transgenic plants and obtained *atprmt5-1* and *atprmt5-2* homozygous mutant plants (Pei et al., 2007; Supplemental Figures S1 and S2). After WT, *atprmt5-1*, *atprmt5-2*, *AtPRMT5*-OE1, and *AtPRMT5*-OE2 seedlings were grown on 1/2 MS medium with or without Cd^{2+} for 14 days, the root lengths of the seedlings were analyzed. As shown in Figure 1E, the root lengths of *atprmt5-1* and *atprmt5-2* were inhibited under Cd^{2+} -stress conditions. By contrast, the phenotype of 35S::*AtPRMT5* plants has been restored (Figure 1, E and F). The expression of *AtPRMT5* (Figure 1E, Heat map) was substantially positive association with root length. Given that root development was affected in the *atprmt5* mutants without Cd^{2+} stress, we analyzed the proportion of root lengths of seedlings treated with Cd^{2+} compared with those that were not treated with Cd^{2+} (Figure 1G). The root lengths of WT plants grown on medium containing 80 μM CdCl_2 were 20%–30% of the plants grown on normal medium, while the root lengths of *AtPRMT5*-OE plants were 30%–40% of the plants grown on medium without Cd^{2+} , and *atprmt5* mutants showed higher Cd^{2+} sensitivity than WT plants. The result was consistent with the above phenotypic observation. Thus, *AtLCD* and *AtPRMT5* play vital roles in response to Cd^{2+} stress in Arabidopsis.

AtPRMT5-mediated methylation of AtLCD at Arg-83 increases the AtLCD activity and H_2S production

Based on the above results and our research on the functions of these two genes over the years (Pei et al., 2007;

Chen et al., 2015; Fang et al., 2017; Zhao et al., 2018), we hypothesized that there was an interaction between *AtPRMT5* and H_2S signals in the Cd^{2+} -stress response. Consequently, H_2S production was examined in WT, *AtPRMT5*-OE plants and *atprmt5* mutants using the H_2S probe 7-azido-4-methylcoumarin (AzMC) (Figure 2, A and B) and methylene blue (Figure 2C). The H_2S contents of *atprmt5-1* and *atprmt5-2* mutants exhibited obvious decreases, whereas the H_2S contents of *AtPRMT5*-OE plants significantly increased compared with the WT.

To further explore the reason for *AtPRMT5* having an effect on the H_2S content, the transcript level of *AtLCD* and its protein expression was determined in WT and *atprmt5* mutant plants. The *AtLCD* expression level and *AtLCD* protein level did not substantially change in *atprmt5* plants (Figure 2, D–F). *PRMT5* can methylate histone H4, H2A, and RNA processing factors. Is *AtLCD* a substrate of *AtPRMT5*? To test this hypothesis, recombinant protein *AtPRMT5* was incubated with *AtLCD* in the presence of the methyl donor *S*-adenosyl-L-[methyl- ^3H] Met for 2 h (Supplemental Figure S4). SM-like protein LSM4, which had been identified as a methyltransferase substrate previously (Zhang et al., 2011), served as a positive control. The autoradiography results showed that the methylation of *AtLCD* was mediated by *AtPRMT5* (Figure 2G). Thus, *AtLCD* is indeed a substrate of *AtPRMT5*. Next, we determined whether the activity of *AtLCD* was affected by *AtPRMT5*-mediated methylation. To answer this question, the Cys desulfhydrase activity of methylated-*AtLCD* via *AtPRMT5* was determined. The methylation mediated by *AtPRMT5* increased *AtLCD* activity significantly (Figure 2H). We further examined *AtLCD* activity in *atprmt5* mutants and *AtPRMT5*-OE transgenic plants. Consistent with the results in vitro, *AtLCD* activities were lower in *atprmt5-1* and *atprmt5-2* mutants, but higher in *AtPRMT5*-OE plants compared with in WT (Figure 2I). Thus, the reduced H_2S content in *atprmt5* plants may be due to a reduced *AtLCD* activity caused by weakened *AtPRMT5*-mediated methylation in Arabidopsis.

Theoretically, 30 Arg residues in the *AtLCD* protein are putative target sites of methylation mediated by *AtPRMT5* (Supplemental Figure S5A). A mass spectrometric analysis of recombinant protein His-*AtLCD* treated with the His-TF-*AtPRMT5* protein in the presence of *S*-adenosyl-L-methionine (SAM) was carried out, and Arg-83 was identified as a very probable methylated residue (Supplemental Figure S5B). Thus, to further verify the methylation of *AtLCD* at

Figure 1 (Continued)

bar, 2 cm. C, Root lengths of seedlings at 14 days. Error bars represent SEs, $n \geq 10$. The heat map displays *AtLCD* expression in WT, *atlcd*, *AtLCD*-OE1, and *AtLCD*-OE2 seedlings, and is based on the RT-qPCR data shown in Supplemental Figures S1 and S2. D, RT-qPCR analysis of the *AtPRMT5* gene in WT with (gray column) or without (black column) Cd^{2+} stress. Error bars represent SEs, $n = 3$. E and F, Analysis of the Cd^{2+} tolerance of WT, *atprmt5-1*, *atprmt5-2*, *AtPRMT5*-OE1, and *AtPRMT5*-OE2 seedlings grown on 1/2 MS medium. E, Phenotypes of seedlings grown on medium without (top panels) or with (bottom panels) 80 μM CdCl_2 for 14 days. The heat map displays the *AtPRMT5* expression in WT, *atprmt5-1*, *atprmt5-2*, *AtPRMT5*-OE1, and *AtPRMT5*-OE2 seedlings based on the RT-qPCR data shown in Supplemental Figures S1 and S2. Scale bar, 2 cm. F, Root lengths of seedlings at 14 days. Error bars represent SEs, $n \geq 10$. G, Root lengths relative to controls of seedlings grown on 1/2 MS medium for 14 days. Error bars represent SEs, $n = 3$. All the data are means \pm SE. Experiments were performed three times with similar results. Different letters indicate significant differences (one-way ANOVA test, $P < 0.05$). * and ** represent significant difference ($P < 0.05$) and extremely significant difference ($P < 0.01$), respectively.

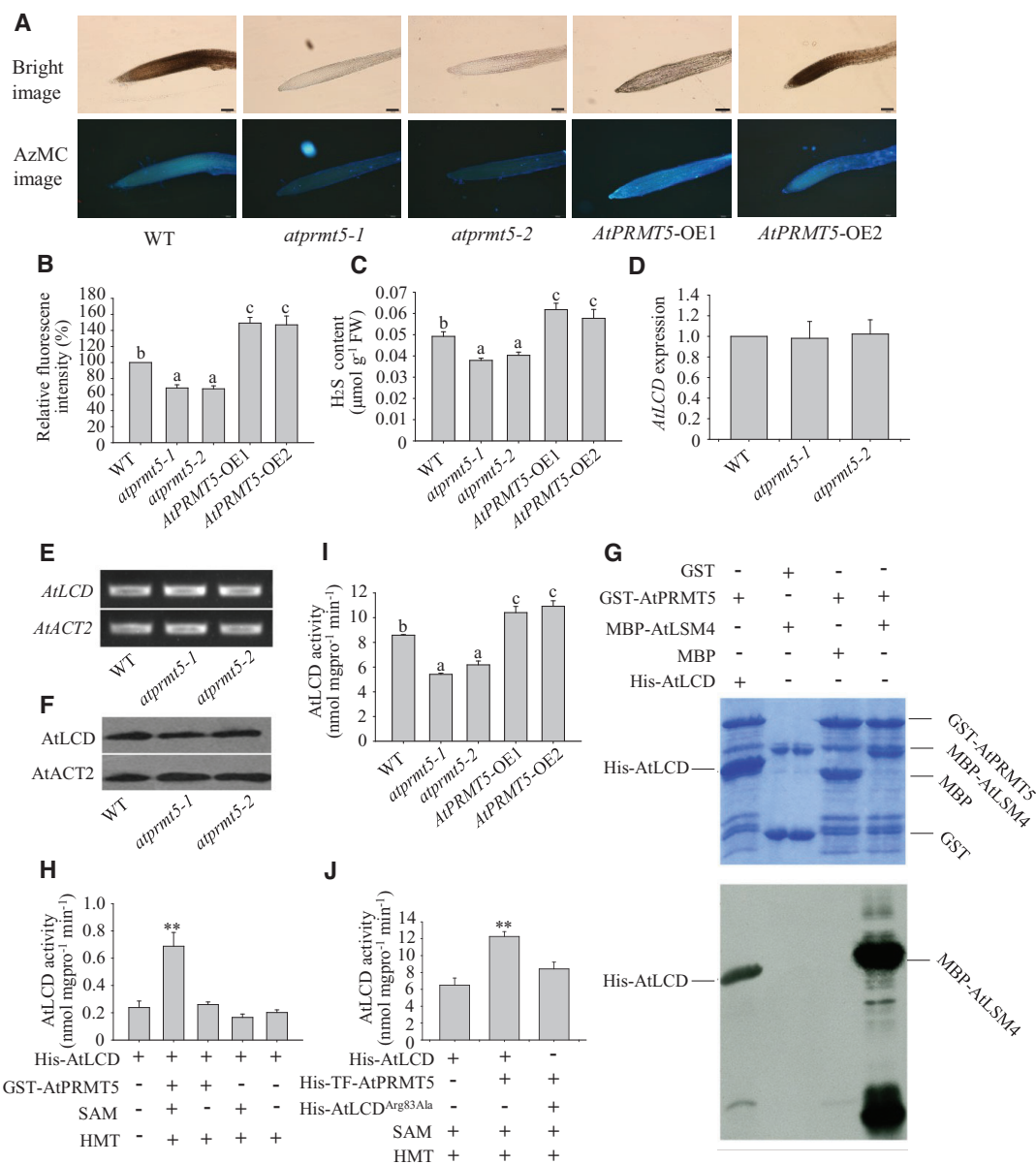


Figure 2 AtPRMT5 methylates AtLCD at Arg-83 and increases its activity. A–C, Analysis of the H₂S contents in WT, *atprmt5-1*, *atprmt5-2*, *AtPRMT5-OE1*, and *AtPRMT5-OE2* seedlings. A, Analysis of the H₂S contents in 14-day-old seedlings using the AzMC probe. Scale bar, 100 μm. B, Analysis of fluorescence density using ImageJ2x. C, Analysis of the H₂S contents in 14-day-old seedlings using methylene blue methods. D and E, The transcriptional levels of *AtLCD* in WT, *atprmt5-1*, and *atprmt5-2* plants as assessed by RT-qPCR (D) and RT-PCR (E) using *AtACT2* as the internal control. F, Immunoblot analysis of *AtLCD* in 14-day-old seedlings. *AtACT2* was used as the internal control. G, Methylation analysis of His-AtLCD catalyzed by GST-AtPRMT5. Recombinant proteins GST-AtPRMT5 and His-AtLCD were incubated in the presence of the methyl donor S-adenosyl-L-[methyl-³H] at 30°C for 2 h. Coomassie bright blue-stained gel is shown in the top panel and the autoradiograph of the gel is shown in the bottom panel. H, Activity analysis of methylated His-AtLCD catalyzed by GST-AtPRMT5. I, Activity analysis of *AtLCD* in WT, *atprmt5-1*, *atprmt5-2*, *AtPRMT5-OE1*, and *AtPRMT5-OE2* plants grown on 1/2 MS medium for 14 days. J, Activity analysis of methylated His-AtLCD and His-AtLCD^{Arg83Ala} proteins catalyzed by His-TF-AtPRMT5. All the data are means ± SE (*n* = 3). Experiments were performed three times with similar results. Different letters indicate significant differences (one-way ANOVA test, *P* < 0.05). * and ** represent significant difference (*P* < 0.05) and extremely significant difference (*P* < 0.01), respectively.

Arg 83 and determine whether the Arg-83 residue was required for increasing the *AtLCD* activity mediated by *AtPRMT5*, we determined the activity of *AtLCD* mutated at Arg-83 to form Ala. *AtLCD*^{Arg83Ala} showed an obvious lower activity level compared with that of *AtLCD* after being treated with *AtPRMT5* (Figure 2).

AtPRMT5 interacts with *AtLCD* in vitro and in vivo
 PRMT5 can methylate different substrates, including histones and non-histones (Bedford and Clarke, 2009; Liu et al., 2010). As a binding partner, PRMT5 mediates SREBP1a methylation and promotes transcriptional activity during the process of metabolic reprogramming in cancer cells

(Liu et al., 2016b). PRMT5 interacts directly and mediates the methylation of DUSP14, which is involved in T-cell receptor signaling (Yang et al., 2018). To investigate the relationship between AtPRMT5 and AtLCD, subcellular localization assays with AtPRMT5 and AtLCD were performed in *N. benthamiana* epidermal cells. The merged yellow fluorescence showed that both AtPRMT5 and AtLCD localized to the nucleus (Figure 3A). Then, we performed bimolecular fluorescence complementation (BiFC) assays to determine the interaction between AtPRMT5 and AtLCD. Protein interaction (green fluorescence) was observed when cotransforming nYFP-AtLCD and cCFP-AtPRMT5 or cCFP-AtLCD and nYFP-AtPRMT5 constructs, whereas no green fluorescent signal was detected in *N. benthamiana* cells cotransformed with AtLCD and cCFP-GUS or AtPRMT5 and cCFP-GUS (Figure 3B). In addition, the merged yellow fluorescence indicated that the interaction occurs in the nucleus. The co-immunoprecipitation (Co-IP) assay was used for determining interactions between AtLCD and AtPRMT5 in vivo (Figure 3C). Protein extracts from WT plants were precipitated using an anti-AtLCD antibody, then the precipitate was examined using anti-AtPRMT5 and anti-AtLCD antibodies. The results confirmed that AtLCD interacted with AtPRMT5 in vivo. Furthermore, we purified the recombinant protein His-TF-AtPRMT5 and incubated it with protein extracts of WT seedlings to examine their interaction in vitro. Again, the pull-down results provide evidence of an

interaction between AtPRMT5 and AtLCD (Figure 3D). Thus, AtPRMT5 appears to physically interact with AtLCD.

AtLCD acts downstream of AtPRMT5 in response to Cd²⁺ stress

To further investigate the genetic interaction relationship of AtPRMT5 and AtLCD in response to Cd²⁺ stress, the *atprmt5-2 atlcd* homozygous double-mutant was generated by crossing *atprmt5-2* with *atlcd* (Supplemental Figure S6). Then WT, *atlcd*, *atprmt5-2*, and *atprmt5-2 atlcd* seedlings were grown on 1/2 MS medium with or without Cd²⁺ for 14 days. The growth of *atlcd*, *atprmt5-2*, and *atprmt5-2 atlcd* was inhibited compared with that of the WT under Cd²⁺-stress conditions (Figure 4A). After 14 days, root lengths were also measured. The results indicated that the root length of WT subjected to Cd²⁺ stress was 20%–30% of WT plants not subjected to Cd²⁺ stress. By contrast, the root lengths of *atlcd* and *atprmt5-2 atlcd* plants were reduced to 10%–20% of those grown in medium without Cd²⁺ stress, whereas the *atprmt5-2* mutant exhibited Cd²⁺ sensitivity to a small extent (Figure 4B). The Cd²⁺ sensitivity of the *atprmt5-2 atlcd* double mutant was much like that of the *atlcd* single mutant in response to Cd²⁺ stress, which suggests that AtLCD acts downstream of AtPRMT5.

The amount of Cd²⁺ accumulated in cells is an important factor in plants that display the Cd²⁺ sensitivity phenotype. To determine the Cd²⁺ contents in roots of different

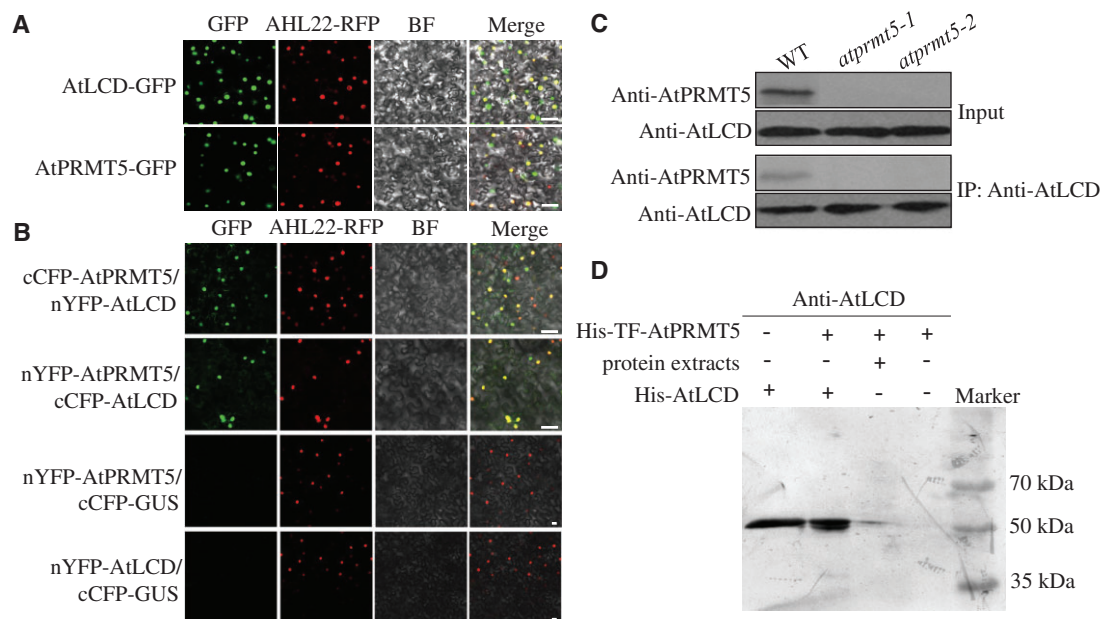


Figure 3 AtPRMT5 interacts with AtLCD. A, Subcellular localizations of the AtLCD and AtPRMT5 proteins. Confocal images of *N. benthamiana* leaf cells harboring the pMDC43-AtLCD or pMDC43-AtPRMT5 constructs. AHL22 was used as an indicator of nuclei; BF, bright field. Scale bar, 10 μ m. B, The interaction between AtLCD and AtPRMT5 in *N. benthamiana* leaves. Pairwise expression of nYFP-AtPRMT5, cCFP-AtPRMT5, nYFP-AtLCD, cCFP-AtLCD, and cCFP-GUS constructs in *N. benthamiana*. AHL22 was used as an indicator of nuclei. BF, bright field. cCFP-GUS was used as a negative control. Scale bar, 10 μ m. C, The combination of AtLCD and AtPRMT5 in 14-day-old Arabidopsis. Protein extracts of WT were immunoprecipitated by anti-AtLCD antibody, and then the precipitates were exposed to anti-AtPRMT5 or anti-AtLCD antibodies. D, Pull-down assays of AtLCD and AtPRMT5. Recombinant protein His-TF-AtPRMT5 binds to Ni-NTA agarose matrix, then incubated with protein extracts from WT plants, the precipitates were immunoblotted with anti-AtLCD antibody.

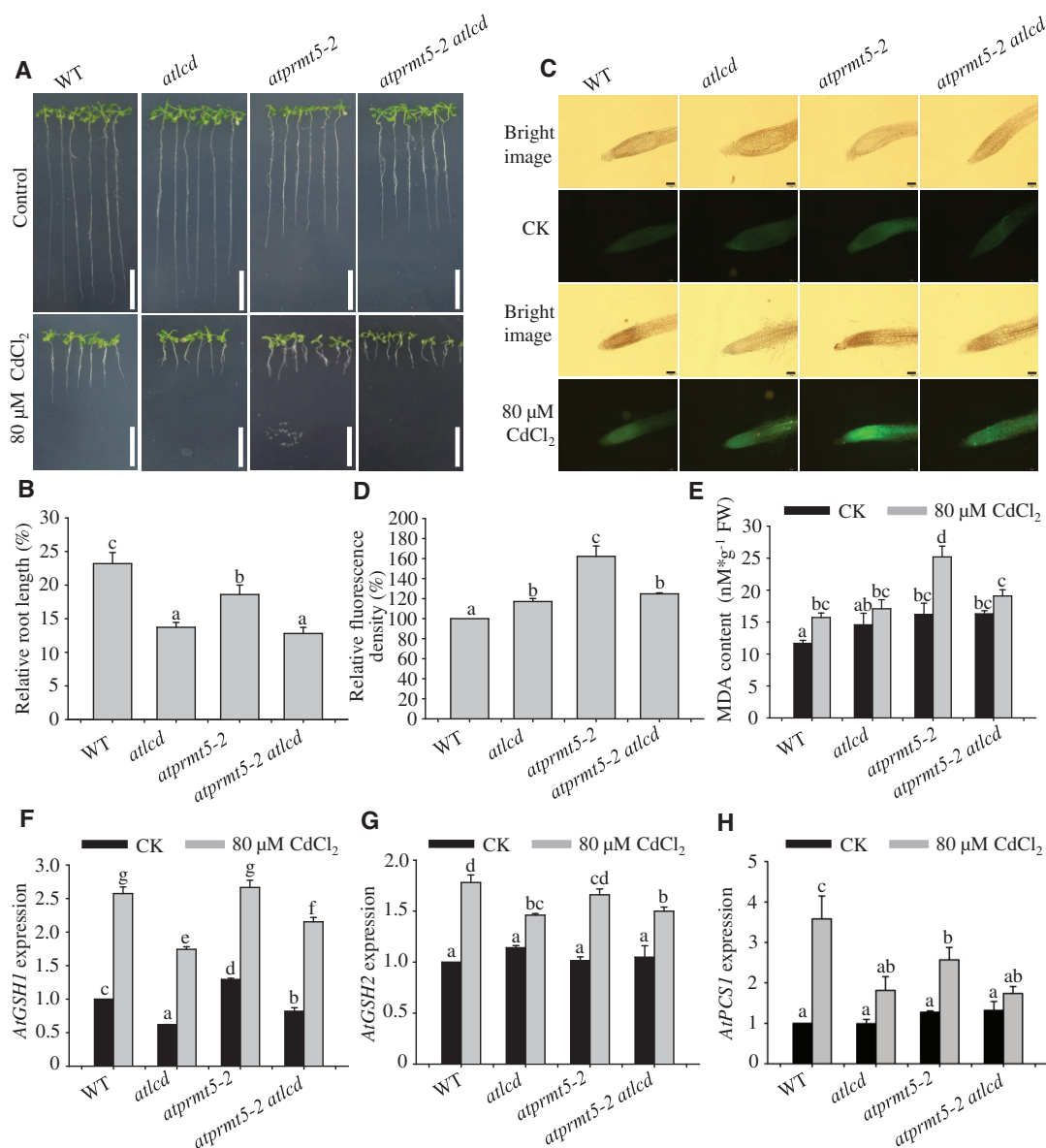


Figure 4 AtLCD acts downstream of AtPRMT5 after exposure to Cd²⁺. A and B, An analysis of the Cd²⁺ tolerance of WT, *atlcd*, *atprmt5-2*, and *atprmt5-2 atlcd* seedlings. A, Phenotypes of seedlings grown on 1/2 MS medium with (bottom panels) or without (top panels) 80 μ M CdCl₂ for 14 days. Scale bar, 2 cm. B, Root lengths relative to controls of 14-day-old seedlings. Error bars represent SEs, $n = 3$. C and D, Roots of WT, *atlcd*, *atprmt5-2*, and *atprmt5-2 atlcd* plants grown on 1/2 MS medium assessed using Leadmium Green AM dye. Roots from 10-day-old seedlings were transferred to 1/2 MS medium with (bottom panels) or without (top panels) 80 μ M CdCl₂ for 5 days, and they were then loaded with Leadmium Green AM dye for 90 min. The images were taken at 10 \times magnification. Scale bar, 100 μ m. Green fluorescence signals indicated that Cd²⁺ and the dye bound. The fluorescence density was analyzed using ImageJ2x software. E, An analysis of the MDA content. The MDA contents were determined at 5 days after 10-day-old seedlings were transferred to the medium supplemented with 80 μ M CdCl₂. F–H, Expression analysis of Cd²⁺ stress-related genes in WT, *atlcd*, *atprmt5-2*, and *atprmt5-2 atlcd* plants. The template RNA was isolated from 10-day-old seedlings treated with 80 μ M CdCl₂ for 12 h. AtACT2 was used as the internal control. All the data are means \pm SE ($n = 3$). Experiments were performed three times with similar results. Different letters indicate significant differences (one-way ANOVA test, $P < 0.05$).

seedlings, a Cd²⁺ probe (LeadmiumTM Green AM dye) was used to detect Cd²⁺ in 10-day-old seedlings transferred to medium with or without 80 μ M CdCl₂ for 5 days. A weak fluorescence signal was observed in WT, whereas stronger and bright green fluorescence signals were observed in the roots of *atprmt5-2* mutant plants exposed to Cd²⁺ stress. The fluorescence intensity in *atprmt5-2 atlcd* plants resembles that of the *atlcd* mutant. The mutants *atprmt5-2 atlcd*

and *atlcd* showed weaker fluorescence signals than in *atprmt5-2* but stronger fluorescence signals than in WT (Figure 4, C and D). To further examine the degree of membrane damage in these plants under Cd²⁺-stress conditions, the malondialdehyde (MDA) content was determined. In general, the higher the MDA content, the higher the membrane damage degree. Similar to the fluorescent probe assay results, we found that Cd²⁺-stress treatments resulted in a

significantly increased MDA level in *atprmt5-2*, as well as slightly increased MDA levels in *atlcd* and *atprmt5-2 atlcd* plants in comparison with WT. The MDA content in *atprmt5-2 atlcd* plants resembled that in the *atlcd* mutant (Figure 4E).

We then examined the expression levels of genes related to Cd²⁺ detoxification in WT, *atlcd*, *atprmt5-2*, and *atprmt5-2 atlcd* plants. Glutathione (GSH) was synthesized by G-glutamylcysteine synthetase and GSH synthetase (Seth et al., 2012). GSH was used as a substrate, and it is catalyzed by phytochelatin (PC) synthase (PCS) to produce PCs (Grill et al., 1989; Thangavel and Long, 2007). PCs bind with cytoplasmic Cd²⁺ to form PC–Cd complexes, which play critical roles in Cd²⁺ detoxification. Thus, Cd²⁺ stress upregulated the expression of *AtGSH1*, *AtGSH2*, and *AtPCS1*. However, the up-regulated gene expression trend was weak in *atlcd*, *atprmt5-2*, and *atprmt5-2 atlcd* mutants compared with

that in WT under Cd²⁺-stress conditions. The induced expression patterns of these genes in *atprmt5-2 atlcd* were more similar to those in *atlcd* than in *atprmt5-2* plants (Figure 4, F–H).

AtPRMT5 regulation of Cd²⁺ tolerance partially depends on H₂S

Does AtPRMT5 improve Cd²⁺ tolerance depending on H₂S? To answer this question, we overexpressed AtPRMT5 in the *atlcd* background, which is defective in H₂S production (Figure 5A). WT, *atlcd*, AtPRMT5-OE, AtPRMT5-OE1/*atlcd*, and AtPRMT5-OE2/*atlcd* plants were cultured on 1/2 MS medium with or without 80 μM CdCl₂ for 14 days to assess Cd²⁺ tolerance. The root lengths of AtPRMT5-OE1/*atlcd* and AtPRMT5-OE2/*atlcd* seedlings in medium containing 80 μM CdCl₂ were inhibited significantly compared with roots of AtPRMT5-OE plants, but they were still longer than those

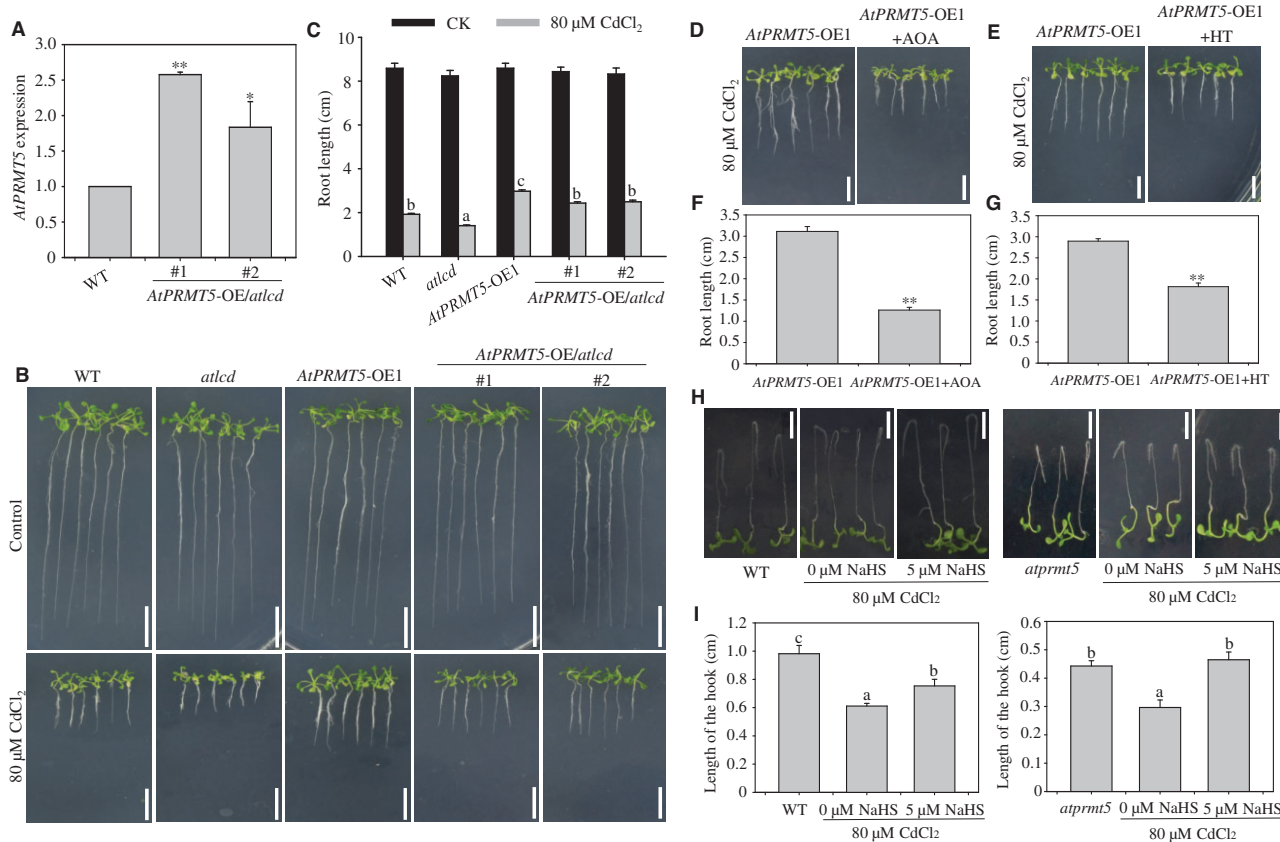


Figure 5 AtPRMT5's regulation of Cd²⁺ tolerance in plants partly depends on H₂S. A, Expression analyses of AtPRMT5 in WT, AtPRMT5-OE1/*atlcd*, and AtPRMT5-OE2/*atlcd* plants as assessed by RT-qPCR. Error bars represent SEs, *n* = 3. B and C, An analysis of the Cd²⁺ tolerance of AtPRMT5-OE plants in an *atlcd* background (AtPRMT5-OE/*atlcd*). B, Phenotypes of WT, *atlcd*, AtPRMT5-OE, AtPRMT5-OE1/*atlcd*, and AtPRMT5-OE2/*atlcd* seedlings grown on 1/2 MS medium with (bottom panels) or without (top panels) 80 μM CdCl₂ for 14 days. Scale bar, 2 cm. C, Root lengths of seedlings at 14 days. Error bars represent SEs, *n* ≥ 12. D–G, Analysis of the Cd²⁺ tolerance of AtPRMT5-OE seedlings in the presence of AOA or HT. D and E, Phenotypes of AtPRMT5-OE1 seedlings grown on 1/2 MS medium containing 80 μM CdCl₂ in the absence (left panels) or presence (right panels) of 50 μM AOA (D) or 100 μM HT (E) for 14 days. Scale bar, 1 cm. F and G, Root lengths of seedlings at 14 days. Error bars represent SEs, *n* ≥ 10. H and I, The alleviation effects of H₂S on WT, *atprmt5-1*, and *atprmt5-2* plants under Cd²⁺-stress conditions. Here, 7-day-old seedlings grown on 1/2 MS medium were fumigated with 5 μM NaHS or not fumigated. The seedlings were then transferred to medium with or without 80 μM CdCl₂ for 72 h. Scale bar, 0.5 cm. The hook lengths of the roots were measured after 72 h. Error bars represent SEs, *n* ≥ 10. All the data are means ± SE. Experiments were performed three times with similar results. Different letters indicate significant differences (one-way ANOVA test, *P* < 0.05). * and ** represent significant difference (*P* < 0.05) and extremely significant difference (*P* < 0.01), respectively.

of *atlcd* plants (Figure 5, B and C). Thus, we speculated that AtPRMT5 ability to enhance Cd²⁺ tolerance in plants was partly dependent on AtLCD.

To further provide evidence that AtPRMT5-mediated AtLCD methylation elevates H₂S production to bolster the Cd²⁺ tolerance in Arabidopsis, root lengths of AtPRMT5-OE1 and AtPRMT5-OE2 seedlings grown on Cd²⁺ stress medium containing either hypotaurine (HT) or aminooxyacetic acid (AOA) were determined. The half-inhibition concentrations of AOA and HT were screened for in preliminary experiments (Supplemental Figures S7 and S8). The root lengths of AtPRMT5-OE1 and AtPRMT5-OE2 seedlings were significantly inhibited when grown in medium supplemented with either HT or AOA (Figure 5, D–G and Supplemental Figure S9). Thus, the reduction in H₂S significantly weakened the promotive role of AtPRMT5 in increasing the Cd²⁺ tolerance of plants.

Furthermore, we performed root-tip bending experiments. We used 5 μM NaHS solution (H₂S donor, Zhao et al., 2001) to fumigate WT and *atprmt5* plants and then transferred the seedlings to medium containing 80 μM CdCl₂ for 72 h. Afterward, the hooks of the roots were observed and measured. H₂S significantly reduced the inhibitory effects of Cd²⁺ on seedling root tips in WT and the *atprmt5* mutants (Figure 5, H and I). These pharmacological experiments suggested that H₂S played a critical role in the process of AtPRMT5-mediated Cd²⁺ tolerance.

Discussion

In this study, we propose a mechanism by which H₂S signaling is enhanced by the protein methylation of AtLCD at Arg-83 mediated by AtPRMT5 during Cd²⁺ stress responses in Arabidopsis (Figure 6).

PRMT5 was involved in the regulation of plant growth and development, multiple stress responses, and the regulation of gene expression mainly by affecting histone methylation. Based on our previous research and other reports, the level of H4R3me2 in the promoter of *AtFLC* decreases in the *atprmt5* mutant, which in turn increases *AtFLC* expression and regulates flowering in Arabidopsis (Pei et al., 2007; Wang et al., 2007; Schmitz et al., 2008). The repressed shoot regeneration phenotype of the *atprmt5* mutant is caused by the decrease in H4R3me2 in the *AtKRP* promoter region, which results in upregulated *AtKRP* expression (Liu et al., 2016a). Similar AtPRMT5 roles have been found in normal shoot apical meristem growth maintenance (Yue et al., 2013), proline accumulation (Fu et al., 2018), Ca²⁺ signaling responses (Fu et al., 2013), and root stem cell maintenance (Li et al., 2016). Furthermore, PRMT5-mediated methylation of the small nuclear ribonucleoprotein components of Sm protein and spliceosome complex LSM4 regulates mRNA alternative splicing, which affects growth-, development-, and stress-responsive genes in plants (Meister et al., 2001; Deng et al., 2010). This strongly implied that histone methylation modifications mediated by AtPRMT5 have evolutionarily conserved functions in regulating different biological

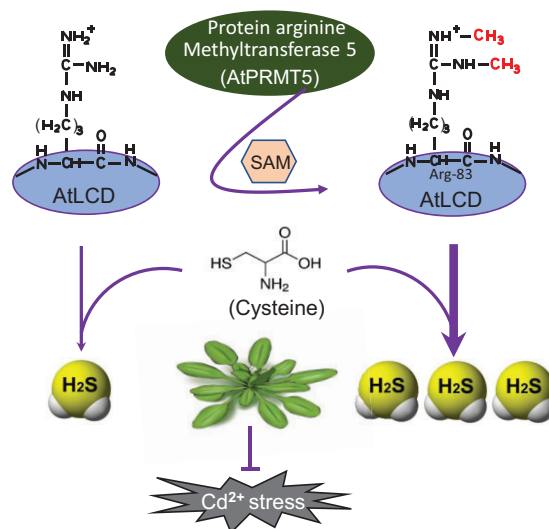


Figure 6 A model of AtPRMT5 regulation of AtLCD activity that results in H₂S production after exposure to Cd²⁺ in Arabidopsis. AtPRMT5-mediated methylation of AtLCD at Arg-83 increases the AtLCD activity and H₂S production, which strengthens Cd²⁺ tolerance.

processes. According to the literature, PRMT5 regulates diverse biological processes mainly through histone and pre-mRNA splicing-related protein (Sanchez et al., 2010; Zhang et al., 2011; Liu et al., 2016a). To date, there have been no reports that PRMT5 uses enzymatic proteins as direct substrates to regulate its activity.

In this study, an interaction between AtLCD and AtPRMT5 in response to Cd²⁺ stress was identified (Figure 1). The H₂S content of *atprmt5* mutant plants decreased (Figure 2, A–C), but the transcriptional and translational levels of AtLCD did not substantially change (Figure 2, D–F). Therefore, we have speculated that AtPRMT5 uses AtLCD as a substrate and regulates its activity through methylation modifications. The result showed that AtPRMT5 has the ability to methylate enzymatic proteins and regulate their activities, in addition to methylating histone and spliceosome-related protein. This is a previously uncharacterized pathway through which AtPRMT5 can regulate plant physiological processes and environmental responses.

H₂S participates in the regulation of Cd²⁺ tolerance in plants. Exogenous H₂S enhances the tolerance to Cd²⁺ by affecting antioxidant enzymes, ROS, and the absorption and transport of heavy metal ions (Sun et al., 2013; Ali et al., 2014; Mostofa et al., 2015). However, the regulatory mechanisms involved in endogenous H₂S generation are still poorly understood. Cd²⁺ stress induces the expression of *AtLCD* and the production of H₂S (Zhang et al., 2015; Qiao et al., 2016). However, the regulatory mechanism is still unknown. Because LCD is crucial for H₂S generation, the regulation of its expression and activity has attracted great interest. Here, we showed that the AtPRMT5-mediated methylation of AtLCD increased its activity and H₂S production, thus bolstering Cd²⁺ tolerance in Arabidopsis. This represents an

important pathway for the regulation of endogenous H₂S generation.

L- and D-Cys can be used as substrates and are catalyzed by LCD and DCD, respectively, to generate H₂S in plants. The L-type amino acids are the main forms in plants, whereas the D-type free amino acids represent only 0.5%–3% of the former. The concentration of L-Cys is 10 μM in plant cells, whereas the concentration of D-Cys is too low to be accurately determined (Riemenschneider et al., 2005). Purified protein BL21 (LCD) degrades L-Cys to generate H₂S, with a H₂S-production rate that is 1.07 times that of the control, whereas purified protein BL21 (DCD) degrades D-Cys into H₂S, with a H₂S-production rate this is 7.2 times that of the control. Thus, DCD exhibits a higher catalytic activity compared with LCD (Shen et al., 2012). Because of the lower D-Cys content, whether DCD could decompose D-Cys to H₂S in plant cells has been ignored. The posttranslational modifications of DCD will be explored in a future study.

Here, we demonstrated that AtLCD acts downstream of AtPRMT5 in response to Cd²⁺ stress in Arabidopsis. The Cd²⁺ sensitivity of the *atprmt5-2 atlcd* double-mutant plants was similar to that of the *atlcd* single mutant (Figure 4, A and B). In addition, the lower Cd²⁺ tolerance of *AtPRMT5-OE/atlcd* plants compared with that of *AtPRMT5-OE* plants further confirmed the conclusion (Figure 5, B and C). However, the Cd²⁺ sensitivity of *AtPRMT5-OE/atlcd* plants was comparable with that of WT and was lower than that of the *atlcd* mutant. Consequently, we speculated that AtPRMT5 partly depends on the H₂S pathway to increase Cd²⁺ tolerance in plants.

AtPRMT5 and AtLCD affected the expression levels of genes involved in Cd²⁺ detoxification. Under Cd²⁺-stress conditions, the expression levels of *AtGSH1/2*, key genes of GSH synthesis, were significantly lower in the *atlcd* and *atprmt5 atlcd* mutant plants than in WT. The same trend was found for *AtPCS1* expression (Figure 4, F–H). These data supported that AtPRMT5 acts upstream of AtLCD in the regulation of PC biosynthesis. Moreover, we further examined the Cd²⁺ contents in the mutant lines. The *atlcd* and *atprmt5-2 atlcd* mutant plants had higher Cd²⁺ contents than the WT, but they had lower Cd²⁺ contents than the *atprmt5* mutant (Figure 4, C and D). In addition, the *atprmt5* mutant exhibited a stronger Cd²⁺ tolerance than *atlcd* and *atprmt5 atlcd* mutant plants (Figure 4, A and B). We speculated that cytoplasmic Cd²⁺ in the *atprmt5* mutant might be transported to the vacuole by metal ion transporters, thereby enhancing Cd²⁺ tolerance in plants. These data also supported a role for H₂S signaling downstream of AtPRMT5.

AtPRMT5 is an activation regulator of AtLCD in Arabidopsis. The AtPRMT5-mediated methylation of AtLCD increases its activity and enhances H₂S production, thereby improving Cd²⁺ tolerance. Our study provides further insights into the biological functions of AtPRMT5 in plants and the study of Arg methylation. In addition, we present a mechanism for endogenous H₂S production and establish a

link between methylation modifications and the regulation of Cd²⁺ tolerance in plants.

Materials and methods

Plant materials and growth conditions

The genetic background of Arabidopsis (*Arabidopsis thaliana*) used in this study was Colombia-0. The T-DNA insert mutants *atprmt5-1* (SALK_065814) and *atprmt5-2* (SALK_095085) were used. Seeds of *atlcd* (SALK_082099) were ordered from the Arabidopsis Biological Resource Center (<http://www.arabidopsis.org/abrc/>) and had been characterized previously (Fang et al., 2017). 35S::AtLCD transgenic plants were constructed in our laboratory. We identified and obtained *atprmt5-2 atlcd* homozygous double-mutants through crosses. Further details can be found in the Supplemental Data.

Seeds were disinfected in 75% (v/v) ethanol for 30 s, followed by 6% (v/v) NaClO for 10 min. Finally, seeds were washed five times with sterile water, for 5 min each time. They were sown in 1/2 MS medium with or without 80 μM CdCl₂ (1% [w/v] sucrose and 1% [w/v] agarose, pH 5.8), then vernalization occurred at 4°C over 3 days under dark conditions. Root lengths of seedlings grown in a greenhouse (at 23°C and 60% relative humidity, with 16-h/8-h light/dark and 160 μE·m⁻²·s⁻¹) were measured after 14 days.

To evaluate the effect of sodium hydrosulfide (NaHS, a H₂S donor, Zhao et al., 2001), HT (a H₂S scavenger, Ortega et al., 2008), and AOA (a Cys desulfhydrase inhibitor, Bianca et al., 2009) on Cd²⁺ sensitivity, 14-day-old seedlings were sown on 1/2 MS medium containing Cd²⁺ in the absence or presence of HT or AOA. Seedlings root lengths were recorded after 14 days. For the root tip bending experiment, 7-day-old seedlings were transferred to medium containing 5 μM NaHS for 24 h, and then, they were exposed to 80 μM CdCl₂ for 72 h. Seedling root lengths were measured.

Plant expression vector construction and generation of transgenic plants

The coding DNA sequence of *AtPRMT5* was amplified from Arabidopsis cDNA. The obtained cDNA fragment was ligated into the *Bam*HI and *Eco*RI sites of XF348, which was provided by Prof. Xiaofeng Cao, to generate the XF348-*AtPRMT5* expression vector. Agrobacterium strain GV3101, carrying XF348-*AtPRMT5*, was introduced into WT and *atlcd* plants by floral dipping (Clough and Bent, 1998). The T3 generation of homozygous plants obtained was used for further experiments. All the primers used in this study are listed in Supplemental Table S1.

Expression and purification of recombinant proteins

The coding region of *AtLCD* was amplified and ligated into pET28a vector (Novagen, Malaysia). The coding region of *AtPRMT5* was amplified and inserted into pCold-TF (TaKaRa, Japan) and pGEX-4T-1 vector (GE Healthcare, USA), respectively. For site-mutated *AtLCD*, primers with

corresponding mutated sites were designed. Recombinant plasmid pET28a-LCD was used as the template for PCR amplification and primers used are listed in [Supplemental Table S1](#). The above PCR products were used for bridge PCR reaction to obtain *AtLCD*^{Arg83Ala}. Then *AtLCD*^{Arg83Ala} gene was ligated into pET28a vector. Constructed plasmids were successfully transformed into BL21 (DE3) to express fusion proteins. The proteins were purified using Ni-NTA Sefnase Resin (Sangon, China) or GST-Sefnase Resin in accordance with the manufacturer's instructions.

BiFC and subcellular localization assay

BiFC methods have been described previously in detail ([Walter et al., 2004](#)). Briefly, to perform subcellular localization and BiFC assays, coding sequences of *AtLCD* and *AtPRMT5* were amplified and cloned independently into the pMDC43 Gateway vector, provided by Liyu Huang (School of Agriculture, Yunnan University), as well as the pNYFP and pCCFP Gateway vectors, provided by Yongfu Fu (Institute of Crop Science, Chinese Academy of Agricultural Sciences). The constructed plasmids were transformed into EHA105 and co-transformed into the leaves of 3-week-old *Nicotiana benthamiana* (*N. benthamiana*) leaves were cultured under the conditions of 16-h/8-h light/dark for 72 h in a greenhouse after infiltration. Fluorescence signals were detected and photographed using confocal laser scanning microscopy (ZEISS, Germany). Excitation and emission wavelengths of GFP are 488/493 to 598 and those of RFP are 561/595 to 670. AHL22-RFP showed nuclear localization ([Xiao et al. 2009](#)). The *N. benthamiana* leaves were transformed with nYFP-*AtPRMT5*/cCFP-GUS and nYFP-*AtLCD*/cCFP-GUS as negative controls.

Pull-down assay

The 14-day-old *Arabidopsis* seedlings were ground in liquid nitrogen and suspended in 1 mL extraction buffer (containing 50 mM PBS pH 7.0, 150 mM NaCl, 0.1% Triton X-100, 1 mM PMSF, and 1× proteinase inhibitor cocktail). Protein extracts of WT plants were centrifuged at 12,000 g at 4°C for 30 min for later experiments. The expression and purification of the His-TF-*AtPRMT5* protein were performed with Ni-NTA agarose beads (Sangon, China) in a 10-mM HEPES buffer using an ultrafiltration device. After ultrafiltration, the His-TF-*AtPRMT5* recombinant protein was bound with pre-treated Ni-NTA agarose beads for 1 h. The unbound proteins were removed by washing three times with solution A (20 mM Tris-Cl, pH 7.5), and then, protein extracts of WT were incubated with Ni-NTA agarose beads at 4°C for 20 min. The beads were collected and washed three times with washing buffer (20 mM Tris-Cl, pH 7.0, 0.5 mol/L NaCl) to remove unbound proteins. The resuspended immunoprecipitates were separated using 12% SDS-PAGE and exposed to an anti-*AtLCD* antibody (2,000×).

Co-IP assay

The Co-IP assay was performed in accordance with previous methods ([Shang et al., 2010](#)). The 14-day-old *Arabidopsis*

seedlings were ground in liquid nitrogen and suspended with 1 mL extraction buffer (containing 50 mM PBS pH 7.0, 150 mM NaCl, 0.1% Triton X-100, 1 mM PMSF, and 1× protease inhibitor cocktail). The protein extracts of WT were centrifuged at 12,000 g at 4°C for 30 min. After pre-incubation with protein G, an anti-*AtLCD* antibody was added and the samples were rotated gently at 4°C overnight. Then, protein G was added at 4°C for 3 h. The beads were collected and washed three times with washing buffer (PBS pH 7.0, 150 mM NaCl, and 0.1% Triton X-100). The precipitates were separated using 12% SDS-PAGE and exposed to an anti-*AtLCD* antibody (2,000×) or anti-*AtPRMT5* antibody (5,000×).

Determination of H₂S contents

The H₂S contents of 14-day-old *Arabidopsis* seedlings grown in 1/2 MS medium were assayed in accordance with previous methods ([Fang et al., 2017](#)). In addition, the H₂S fluorescence probe (Sigma-Aldrich) was used to determine the H₂S contents of 14-day-old seedlings. Seedlings were incubated in 20 mM HEPES-NaOH buffer (pH 7.5) containing 10 μM AzMc probes for 20 min. Then, seedlings were washed three times with 20 mM HEPES for 15 min each time. Fluorescence signals were observed using a fluorescence microscope, and fluorescence intensities were analyzed using ImageJ2x (Rawak Software Inc., Stuttgart, Germany). Samples were excited at 360–370 nm and emission was recorded at 420 nm.

Determination of *AtLCD* activity

The *AtLCD* activity levels were determined in accordance with previously reported methods ([Fang et al., 2017](#)).

Analysis of methyltransferase activity in vitro

The determination of methyltransferase activity was performed as described previously ([Pei et al., 2007](#)). Recombinant plasmid GST-*AtPRMT5* was transformed into BL21 (DE3) to express the fusion protein. Then, purified GST-*AtPRMT5* protein and His-*AtLCD* protein were incubated with methyl donor *S*-adenosyl-L-[methyl-³H] Met (Amersham Biosciences, USA) in HMT buffer (20 mM Tris-HCl, pH 8.0, 4 mM EDTA, 1 mM PMSF, and 0.5 mM DTT) at 30°C for 1–3 h. The proteins were separated using 12% SDS-PAGE and Coomassie bright blue staining for visualization. Gels were dried and exposed to Kodak Biomax MS film.

The purified proteins His-TF-*AtPRMT5* and His-*AtLCD* were treated with methyl donor SAM (Solarbio, China) in HMT buffer at 30°C for 2 h. The reaction mixtures were used for the determination of *AtLCD* activity.

Liquid chromatograph/mass spectrometry/mass spectrometry analysis

Purified His-*AtLCD* protein was treated with His-TF-*AtPRMT5* protein at 30°C for 2 h in the presence of the methyl donor SAM. After the addition of six volumes of 10% trichloroacetic acid/acetone overnight, the proteins

were precipitated by centrifugation at 4°C and 14,000 g for 10 min. The precipitates were washed with 100% acetone and resuspended in 8 M urea in 100 mM Trizma base buffer (pH 8.0). Then, the proteins were reduced, alkylated, and digested with trypsin using the FASP method (Wiśniewski et al., 2009). Tryptic peptides were redissolved in 0.1% formic acid and then, an approximately 200-µg sample was injected into an ACQUITY UPLC M-class high-performance liquid chromatography system (Waters, USA) that was on-line with an Orbitrap Fusion Lumos (Thermo Fisher Scientific, USA). The sample was loaded directly onto the analytical column (nanoEase M/Z HSS C18, 75 µm × 25 cm, Waters) using a mobile phase buffer that consisted of 0.1% formic acid in water (buffer A) and an eluting buffer of 0.1% formic acid in 100% acetonitrile (v/v, buffer B). The gradient was set as 4%–7% buffer B for 3 min, 7%–20% for 20 min, and 20%–30% for 11 min at 600 nL min⁻¹. The peptides were ionized when the spray voltage was 2.2 kV and then, they entered the mass spectrometry system. The mass spectrometry was in a data-dependent acquisition mode and switched automatically between mass spectrometry and mass spectrometry/mass spectrometry acquisition on a 3-s cycle.

All the raw data were analyzed using Proteome Discoverer 2.2 (Thermo Fisher Scientific) with the protein sequences of AtLCD and AtPRMT5. The false discovery rates of proteins and peptides were set to 0.01, and the minimum and maximum lengths of peptides were 6 and 144, respectively. The methylation modification of Cys was designated as the fixation modification, whereas the methionine oxidation and Arg methylation were considered variable modifications. A decoy database search was employed to generate high ($P < 0.01$) and medium ($P < 0.05$) confidence peptide lists.

Measurement of MDA

The MDA content was assayed in accordance with previously published methods (Zhang et al., 2015). Arabidopsis seedlings were homogenized with 5% trichloroacetic acid. The mixtures were centrifuged at 8,000 g for 10 min. The supernatants were mixed with 0.67% thiobarbituric acid. The mixtures were heated at 100°C for 30 min. After centrifugation at 8,000 g for 5 min, the absorbance of the supernatant was measured at 450, 532, and 600 nm.

Analysis of gene expression

The total RNAs from seedlings were extracted using TRIzol (TakaRa, Japan). Reverse transcription reactions were carried out using 5 × All-In-One RT MasterMix (abm, China) in accordance with the instruction manual. Reverse transcription quantitative PCR (RT-qPCR) analysis was performed using an EvaGreen Kit (Biotium, USA). The relative expression levels of target genes were calculated using the 2^{-ΔΔCt} method (Livak and Schmittgen, 2001). AtACT2 (AT3G18780) was the internal reference for RT-PCR and RT-qPCR. For each experiment, at least three independent biological and technical repeats were performed.

Analysis of Cd²⁺ content using Cd²⁺-specific fluorescent probes

At 10 days after germination, Arabidopsis seedlings of different genotypes were transferred to 1/2 MS medium with or without 80 µM CdCl₂ for 5 days. Seedlings were incubated with 0.5% LeadmiumTM Green AM dye (Molecular Probes, Invitrogen, Carlsbad, California, USA) for 1 h at 37°C. Seedlings were washed with washing buffer (0.85% NaCl) three times for 5 min each time. Fluorescence signals were observed under a fluorescence microscope equipped with a specific filter set (excitation at 488 nm and emission at 500–517 nm). The mean fluorescence intensity was quantified using ImageJ2x (Rawak Software Inc.). The experiments were repeated twice.

Statistical analysis

A one-way ANOVA was used for determining statistical significance. Data shown in experiments are mean averages ± standard errors (SEs). * and ** represent significant differences ($P < 0.05$) and extremely significant differences ($P < 0.01$), respectively. All the data were analyzed using SPSS (version 17, IBM SPSS, USA).

Accession numbers

Sequence information used in this study was downloaded from the Arabidopsis Information Resource Centre (<https://www.arabidopsis.org/>). The accession numbers are as follows: AtLCD (AT3G62130), AtPRMT5 (AT4G31120), AtPCS1 (AT5G44070), AtGSH1 (AT4G23100), and AtGSH2 (AT5G27380).

Supplemental data

The following materials are available in the online version of this article.

Supplemental Figure S1. The identification of *atlcd*, *atprmt5-1*, and *atprmt5-2* mutants.

Supplemental Figure S2. The analysis of DNA identification and gene expression in *AtLCD*-OE, *AtPRMT5*-OE plants.

Supplemental Figure S3. The effect of Cd²⁺ on seedlings grown on 1/2 MS medium.

Supplemental Figure S4. The purification and separation of recombinant proteins.

Supplemental Figure S5. Amino acid sequence and mass spectrometry analysis of AtLCD protein.

Supplemental Figure S6. DNA identification of *atprmt5 atlcd* double mutant.

Supplemental Figure S7. The effect of AOA on seedlings grown on 1/2 MS medium containing 80 µM CdCl₂.

Supplemental Figure S8. The effect of HT on seedlings grown on 1/2 MS medium with 80 µM CdCl₂.

Supplemental Figure S9. The analysis of Cd²⁺ tolerance of *AtPRMT5*-OE2 seedlings in the presence of AOA or HT.

Supplemental Table S1. Primers used in this study.

Acknowledgments

We are grateful to Dr Yongfu Fu (Institute of Crop Science, Chinese Academy of Agricultural Sciences) for providing the

BiFC vectors pNYFP-X and pCCFP-X, Dr Liyu Huang (School of Agriculture, Yunnan University) for providing the pMDC43 Gateway vector, and Dr Liang Yang (Westlake Omics [Hangzhou] Biotechnology, Zhejiang Province, China) for mass spectrometric analysis.

Funding

This work was supported by the National Natural Science Foundation of China (31972428 to Yanxi Pei, 32172550 to Zhuping Jin).

Conflict of interest statement. The authors declare that they have no conflict of interest.

References

- Alamri S, Kushwaha BK, Singh VP, Siddiqui MH (2020) Dose dependent differential effects of toxic metal cadmium in tomato roots: role of endogenous hydrogen sulfide. *Ecotoxicol Environ Saf* **203**: 110978
- Ali B, Gill RA, Yang S, Gill MB, Ali S, Rafiq MT, Zhou WJ (2014) Hydrogen sulfide alleviates cadmium-induced morpho-physiological and ultrastructural changes in *Brassica napus*. *Ecotoxicol Environ Saf* **110**: 197–207
- Bedford MT, Clarke SG (2009) Protein arginine methylation in mammals: who, what, and why. *Mol Cell* **33**: 1–13
- Bedford MT, Richard S (2005) Arginine methylation an emerging regulator of protein function. *Mol Cell* **18**: 263–272
- Bianca RDD, Sorrentino R, Maffia P, Mirone V, Imbimbo C, Fusco F, De Palma R, Ignarro LJ, Cirino G (2009) Hydrogen sulfide as a mediator of human corpus cavernosum smooth-muscle relaxation. *Proc Natl Acad Sci USA* **106**: 4513–4518
- Blanc RS, Richard S (2017) Arginine methylation: the coming of age. *Mol Cell* **65**: 8–24
- Buchet JP, Lauwerys R, Roels H, Bernard A, Bruaux P, Claeys F, Ducoffre G, Plaen Pde, Staessen J, Amery A (1990) Renal effects of cadmium body burden of the general population. *Lancet* **336**: 699–702
- Chen J, Wu FH, Shang YT, Wang WH, Hu WJ, Simon M, Liu X, Shangguan ZP, Zheng HL (2015) Hydrogen sulphide improves adaptation of *Zea mays* seedlings to iron deficiency. *J Exp Bot* **66**: 6605–6622
- Chen SS, Jia HL, Wang XF, Shi C, Wang X, Ma PY, Wang J, Ren MJ, Li JS (2020) Hydrogen sulfide positively regulates abscisic acid signaling through persulfidation of SnRK2.6 in guard cells. *Mol Plant* **13**: 732–744
- Clemens S (2006) Evolution and function of phytochelatin synthases. *J Plant Physiol* **163**: 319–332
- Clemens S, Ma JF (2016) Toxic heavy metal and metalloid accumulation in crop plants and foods. *Annu Rev Plant Biol* **67**: 489–512
- Clough SJ, Bent AF (1998) Floral dip: a simplified method for Agrobacterium-mediated transformation of *Arabidopsis thaliana*. *Plant J* **16**: 735–743
- Corpas FJ (2019) Hydrogen sulfide: a new warrior against abiotic stress. *Trends Plant Sci* **24**: 983–988
- Cui WT, Chen HP, Zhu KK, Jin QJ, Xie YJ, Cui J, Xia Y, Zhang J, Shen WB (2014) Cadmium-induced hydrogen sulfide synthesis is involved in cadmium tolerance in *Medicago sativa* by reestablishment of reduced (homo)glutathione and reactive oxygen species homeostasis. *PLoS ONE* **9**: e109669
- Deng X, Gu LF, Liu TC, Lu CY, Lu FL, Lu ZK, Cui P, Pei YX, Wang BC, Hu SN, et al. (2010) Arginine methylation mediated by the Arabidopsis homolog of PRMT5 is essential for proper pre-mRNA splicing. *Proc Natl Acad Sci USA* **107**: 19114–19119
- Fang HH, Liu ZQ, Long YP, Liang YL, Jin ZP, Zhang LP, Liu DM, Li H, Zhai JX, Pei YX (2017) The Ca²⁺/calmodulin2-binding transcription factor TGA3 elevates LCD expression and H₂S production to bolster Cr⁶⁺ tolerance in Arabidopsis. *Plant J* **91**: 1038–1050
- Fan HJ, Zhang ZL, Wang N, Cui Y, Sun H, Liu Y, Wu HL, Zheng SS, Bao SL, Ling HQ (2014) SKB1/PRMT5-mediated histone H4R3 dimethylation of Ib subgroup bHLH genes negatively regulates iron homeostasis in *Arabidopsis thaliana*. *Plant J* **77**: 209–221
- Fu YL, Ma HL, Chen SY, Gu TY, Gong JM (2018) Control of proline accumulation under drought via a novel pathway comprising the histone methylase CAU1 and the transcription factor ANAC055. *J Exp Bot* **69**: 579–588
- Fu YL, Zhang GB, Lv XF, Guan Y, Yi HY, Gong JM (2013) Arabidopsis histone methylase CAU1/PRMT5/SKB1 acts as an epigenetic suppressor of the calcium signaling gene CAS to mediate stomatal closure in response to extracellular calcium. *Plant Cell* **25**: 2878–2891
- Grill E, Löffler S, Winnacker EL, Zenk MH (1989) Phytochelatin, the heavy-metal-binding peptides of plants, are synthesized from glutathione by a specific gamma-glutamylcysteine dipeptidyl transpeptidase (phytochelatin synthase). *Proc Natl Acad Sci USA* **86**: 6838–6842
- Hong S, Song HR, Lutz K, Kerstetter RA, Michael TP, McClung CR (2010) Type II protein arginine methyltransferase 5 (PRMT5) is required for circadian period determination in *Arabidopsis thaliana*. *Proc Natl Acad Sci USA* **107**: 21211–21216
- Hu JL, Yang HJ, Mu JY, Lu TC, Peng JL, Deng X, Kong ZS, Bao SL, Cao XF, Zuo JR (2017) Nitric oxide regulates protein methylation during stress responses in plants. *Mol Cell* **67**: 702–710.e4
- Jiang JL, Ren XM, Li L, Hou RP, Sun W, Jiao CJ, Yang N, Dong YX (2020) H₂S regulation of metabolism in Cucumber in response to salt-stress through transcriptome and proteome analysis. *Front Plant Sci* **11**: 1283
- Jin ZP, Xue AW, Luo YN, Tian BH, Fang HH, Li H, Pei YX (2013) Hydrogen sulfide interacting with abscisic acid in stomatal regulation responses to drought stress in Arabidopsis. *Plant Physiol Biochem* **62**: 41–64
- Li QL, Zhao Y, Yue MH, Xue YB, Bao SL (2016) The protein Arginine methylase 5 (PRMT5/SKB1) gene is required for the maintenance of root stem cells in response to DNA damage. *J Genet Genomics* **43**: 187–197
- Liu CY, Lu FL, Cui X, Cao XF (2010) Histone methylation in higher plants. *Annu Rev Plant Biol* **61**: 395–420
- Liu H, Ma X, Han HN, Hao YJ, Zhang XS (2016a) AtPRMT5 regulates shoot regeneration through mediating histone H4R3 dimethylation on KRPs and pre-mRNA splicing of RKP in Arabidopsis. *Mol Plant* **9**: 1634–1646
- Liu L, Zhao XP, Zhao L, Li JJ, Yang H, Zhu ZP, Liu JJ, Huang G (2016b) Arginine methylation of SREBP1a via PRMT5 promotes de novo lipogenesis and tumor growth. *Cancer Res* **76**: 1260–1272
- Liu ZQ, Li YW, Cao CY, Liang S, Ma YS, Liu X, Pei YX (2019) The role of H₂S in low temperature-induced cucurbitacin C increases in cucumber. *Plant Mol Biol* **99**: 535–544
- Livak KJ, Schmittgen TD (2001) Analysis of relative gene expression data using real-time quantitative PCR and the 2^{-Delta Delta C(T)} Method. *Methods* **25**: 402–408
- Li ZG, Yang SZ, Long WB, Yang GX, Shen ZZ (2013) Hydrogen sulphide may be a novel downstream signal molecule in nitric oxide-induced heat tolerance of maize (*Zea mays* L.) seedlings. *Plant Cell Environ* **36**: 1564–1572
- Luo SL, Tang ZQ, Yu JH, Liao WB, Xie JM, Lv J, Feng Z, Dawdle MM (2020) Hydrogen sulfide negatively regulates CD-induced cell death in cucumber (*Cucumis sativus* L) root tip cells. *BMC Plant Biol* **20**: 480
- Lv WJ, Yang LF, Xu CF, Shi ZQ, Shao JS, Xian M, Chen J (2017) Cadmium disrupts the balance between hydrogen peroxide and superoxide radical by regulating endogenous hydrogen sulfide in the root tip of *Brassica rapa*. *Front Plant Sci* **8**: 232

- Meister G, Eggert C, Bühler D, Brahms H, Kambach C, Fischer U** (2001) Methylation of Sm proteins by a complex containing PRMT5 and the putative U snRNP assembly factor pICln. *Curr Biol* **11**: 1990–1994
- Mostofa MG, Rahman A, Ansary MMU, Watanabe A, Fujita M, Tran LSP** (2015) Hydrogen sulfide modulates cadmium-induced physiological and biochemical responses to alleviate cadmium toxicity in rice. *Sci Rep* **5**: 14078
- Ortega JA, Ortega JM, Julian D** (2008) Hypotaurine and sulfhydryl-containing antioxidants reduce H₂S toxicity in erythrocytes from a marine invertebrate. *J Exp Biol* **211**: 3816–3825
- Papenbrock J, Riemenschneider A, Kamp A, Schulz-Vogt HN, Schmidt A** (2007) Characterization of cysteine-degrading and H₂S-releasing enzymes of higher plants - from the field to the test tube and back. *Plant Biol (Stuttg)* **9**: 582–588
- Pei YX, Niu LF, Lu FL, Liu CY, Zhai JX, Kong XF, Cao XF** (2007) Mutations in the Type II protein arginine methyltransferase AtPRMT5 result in pleiotropic developmental defects in *Arabidopsis*. *Plant Physiol* **144**: 1913–1923
- Qiao ZJ, Jing T, Liu ZQ, Zhang LP, Jin ZP, Liu DM, Pei YX** (2015) H₂S acting as a downstream signaling molecule of SA regulates Cd tolerance in *Arabidopsis*. *Plant and Soil* **393**: 137–146
- Qiao ZJ, Jing T, Jin ZP, Liang YL, Zhang LP, Liu ZQ, Liu DM, Pei YX** (2016) CDPKs enhance Cd tolerance through intensifying H₂S signal in *Arabidopsis thaliana*. *Plant and Soil* **398**: 99–110
- Riemenschneider A, Wegele R, Schmidt A, Papenbrock J** (2005) Isolation and characterization of a D-cysteine desulfhydrase protein from *Arabidopsis thaliana*. *FEBS J* **272**: 1291–1304
- Sanchez SE, Petrillo E, Beckwith EJ, Zhang X, Rugnone ML, Hernando CE, Cuevas JC, Herz MAG, Depetris-Chauvin A, Simpson CG, et al.** (2010) A methyl transferase links the circadian clock to the regulation of alternative splicing. *Nature* **468**: 112–116
- Schmitz RJ, Sung S, Amasino RM** (2008) Histone arginine methylation is required for vernalization-induced epigenetic silencing of FLC in winter-annual *Arabidopsis thaliana*. *Proc Natl Acad Sci USA* **105**: 411–416
- Scuffi D, Álvarez C, Laspina N, Gotor C, Lamattina L, García-Mata C** (2014) Hydrogen sulfide generated by L-cysteine desulfhydrase acts upstream of nitric oxide to modulate abscisic acid-dependent stomatal closure. *Plant Physiol* **166**: 2065–2076
- Seth CS, Remans T, Keunen E, Jozefczak M, Gielen H, Opdenakker K, Weyens N, Vangronsveld J, Cuypers A** (2012) Phytoextraction of toxic metals: a central role for glutathione. *Plant Cell Environ* **35**: 334–346
- Shang Y, Yan L, Liu ZQ, Cao Z, Mei C, Xin Q, Wu FQ, Wang XF, Du SY, Jiang T, et al.** (2010) The Mg-Chelatase H subunit of *Arabidopsis* antagonizes a group of WRKY transcription repressors to relieve ABA responsive genes of inhibition. *Plant Cell* **22**: 1909–1935
- Shen JJ, Qiao ZJ, Xing TJ, Zhang LP, Liang YL, Jin ZP, Yang GD, Wang R, Pei YX** (2012) Cadmium toxicity is alleviated by AtLCD and AtDCD in *Escherichia coli*. *J Appl Microbiol* **113**: 1130–1138
- Shen J, Zhang J, Zhou MJ, Zhou H, Cui BM, Gotor C, Romero LC, Fu L, Yang J, Foyer CH, et al.** (2020) Persulfidation-based modification of cysteine desulfhydrase and the NADPH oxidase RBOHD controls guard cell abscisic acid signaling. *Plant Cell* **32**: 1000–1017
- Sun J, Wang RG, Zhang X, Yu YC, Zhao R, Li ZY, Chen SL** (2013) Hydrogen sulfide alleviates cadmium toxicity through regulations of cadmium transport across the plasma and vacuolar membranes in *Populus euphratica* cells. *Plant Physiol Biochem* **65**: 67–74
- Thangavel P, Long SR** (2007) Changes in phytochelatin and their biosynthetic intermediates in red spruce (*Picea rubens* Sarg.) cell suspension cultures under cadmium and zinc stress. *Plant Cell Tissue Organ Cult* **88**: 201–216
- Walter M, Chaban C, Schütze K, Batistic O, Weckermann K, Näke C, Blazevic D, Grefen C, Schumacher K, Oecking C, et al.** (2004) Visualization of protein interactions in living plant cells using bimolecular fluorescence complementation. *Plant J* **40**: 428–438
- Wang HR, Che YH, Wang ZH, Zhang BN, Huang D, Feng FJ, Ao H** (2021) The multiple effects of hydrogen sulfide on cadmium toxicity in tobacco may be interacted with CaM signal transduction. *J Hazard Mater* **403**: 123651
- Wang R** (2002) Two's company, three's a crowd: can H₂S be the third endogenous gaseous transmitter? *FASEB J* **16**: 1792–1798
- Wang X, Zhang Y, Ma QB, Zhang ZL, Xue YB, Bao SL, Chong K** (2007) SKB1-mediated symmetric dimethylation of histone H4R3 controls flowering time in *Arabidopsis*. *EMBO J* **26**: 1934–1941
- Wiśniewski JR, Zougman A, Nagaraj N, Mann M** (2009) Universal sample preparation method for proteome analysis. *Nat Methods* **6**: 359–362
- Xiao CW, Chen FL, Yu XH, Lin CT, Fu YF** (2009) Over-expression of an AT-hook gene, AHL22, delays flowering and inhibits the elongation of the hypocotyl in *Arabidopsis thaliana*. *Plant Mol Biol* **71**: 39–50
- Yang CY, Chiu LL, Chang CC, Chuang HC, Tan TH** (2018) Induction of DUSP14 ubiquitination by PRMT5-mediated arginine methylation. *FASEB J* **32**: fj201800244RR
- Yue MH, Li QL, Zhang Y, Zhao Y, Zhang ZL, Bao SL** (2013) Histone H4R3 methylation catalyzed by SKB1/PRMT5 is required for maintaining shoot apical meristem. *PLoS ONE* **8**: e83258
- Zhang H, Tang J, Liu XP, Wang Y, Yu W, Peng WY, Fang F, Ma DF, Wei ZJ, Hu LY** (2009) Hydrogen sulfide promotes root organogenesis in *Ipomoea batatas*, *Salix matsudana* and *Glycine max*. *J Integr Plant Biol* **51**: 1086–1094
- Zhang J, Zhou MJ, Ge ZL, Shen J, Zhou C, Gotor C, Romero LC, Duan XL, Liu X, Wu DL, et al.** (2020a) Abscisic acid-triggered guard cell L-cysteine desulfhydrase function and in situ hydrogen sulfide production contributes to heme oxygenase-modulated stomatal closure. *Plant Cell Environ* **43**: 624–636
- Zhang LP, Pei YX, Wang HJ, Jin ZP, Liu ZQ, Qiao ZJ, Fang HH, Zhang YJ** (2015) Hydrogen sulfide alleviates cadmium-induced cell death through restraining ROS accumulation in roots of *Brassica rapa* L. ssp. *pekinensis*. *Oxid Med Cell Longev* **2015**: 804603
- Zhang Q, Cai W, Ji TT, Ye L, Lu YT, Yuan TT** (2020b) WRKY13 enhances cadmium tolerance by promoting D-CYSTEINE DESULFHYDRASE and hydrogen sulfide production. *Plant Physiol* **183**: 345–357
- Zhang ZL, Zhang SP, Zhang Y, Wang X, Li D, Li QL, Yue MH, Li Q, Zhang YE, Xu YY, et al.** (2011) *Arabidopsis* floral initiator SKB1 confers high salt tolerance by regulating transcription and pre-mRNA splicing through altering histone H4R3 and small nuclear ribonucleoprotein LSM4 methylation. *Plant Cell* **23**: 396–411
- Zhao N, Zhu HP, Zhang HL, Sun J, Zhou JC, Deng C, Zhang YH, Zhao R, Zhou XY, Lu CF, et al.** (2018) Hydrogen sulfide mediates K⁺ and Na⁺ homeostasis in the roots of salt-resistant and salt-sensitive poplar species subjected to NaCl stress. *Front Plant Sci* **9**: 1366
- Zhao W, Zhang J, Lu Y, Wang R** (2001) The vasorelaxant effect of H(2)S as a novel endogenous gaseous K(ATP) channel opener. *EMBO J* **20**: 6008–6016
- Zhou ZH, Wang Y, Ye XY, Li ZG** (2018) Signaling molecule hydrogen sulfide improves seed germination and seedling growth of maize (*Zea mays* L.) under high temperature by inducing antioxidant system and osmolyte biosynthesis. *Front Plant Sci* **9**: 1288